Correlations among Spall Void Shape Distributions, Damage Mode and Shock Loading Kinetics

A.D. Brown[1], Q. Pham[2], E.V. Fortin[2], P. Peralta[2], B.M. Patterson[3], J.P. Escobedo Diaz[1], E.K. Cerreta[3], S.N. Luo[4], D. Dennis-Koller[3], D. Byler[3], A. Koskelo[3], X. Xiao[5]

[1]SEIT, The University of New South Wales; Northcott Dr.; Canberra, ACT, 2610, Australia
[2]Arizona State University; 501 E. Tyler Mall; Tempe, AZ, 85287, USA
[3]Los Alamos National Laboratory; Los Alamos, NM, 87545, USA
[4]Peac Institute of Multiscale Sciences; 2nd Section Chuanda Rd.; Chengdu, 610207, China
[5]Argonne National Laboratory; 9700 S. Cass Ave.; Lemont, IL, 60439, USA

ABSTRACT

Three-dimensional X-ray tomography (XRT) provides a non-destructive technique to fully characterize the size, shape, and location of spall damage within shock loaded metals. A shape fitting method using the inertia tensors of individual damage sites was applied to study differences of spall damage development in face-centered-cubic (FCC) and hexagonal-closed-packed (HCP) multicrystals (MC) and for a suite of experiments on high-purity copper to examine the influence of loading kinetics on the spall damage process. Applying a volume weighted average to the best-fit ellipsoidal aspect-ratios allows a quantitative assessment that can be used to determine the extent of spall coalescence present in a shocked metal. It was found that incipient transgranular HCP spall damage nucleates in a lenticular shape and is heavily oriented along particular crystallographic slip directions. Shape distributions indicate a decrease in the tensile loading rate leads to a transition to coalesced damage dominance and that the plastic processes driving void growth are time dependent.

INTRODUCTION

Spall damage is the primary damage mode in metallic materials subject to shock loading and occurs when tensile release waves from an impact interact, leading to stresses that exceed the tensile strength of the material. This, in turn, results in void nucleation, growth, and coalescence in the form of a spall plane [1-3]. The evolution of dynamic spall damage in materials subjected to high stress and strain rate conditions has been widely studied due to the complexity of the process, which is affected by the microstructure along with intrinsic and extrinsic defects [4-18] and the shock wave pulse shape or loading profile [4, 19-21]. Recent studies on shocked copper have made progress in linking the microstructure to damage development [7-18], however, determining the mechanisms governing the spall damage process also requires careful consideration of the loading profile for a complete analysis on damage development [19-21]. Spall damage has been widely studied in FCC metals [4, 7-23], but there are limited studies on the damage development in HCP metals [24-28], specifically pure HCP metals such as titanium. The spall damage studies found in [24-28] are limited to Ti alloys.

There is a known statistical preference for spall damage being present at grain boundaries (GBs) with misorientation angles between 25^{o} and 50^{o} in incipiently spalled copper of varying thermomechanical histories [8-10, 14]. It is also widely accepted that special $\Sigma 1$ and $\Sigma 3$ GBs are resistant to void nucleation [7-16]. The inclination of GBs with respect to the shock direction have been studied by Fensin et al. [15] and Krishnan et al. [14]; concluding that GBs oriented 67^{o} to 90^{o} from the shock direction in 2D and adjacent GBs with high Taylor factor mismatches are most likely to experience spall nucleation and

growth, respectively. The preference between inter- and transgranular damage present within incipiently spalled copper polycrystals (PCs) of varying thermomechanical histories using 3D XRT has been extensively investigated by Brown et al. [9, 10, 18, 19] and Yang et al. [22, 23]. It was concluded that plastic pre-strain from cold rolling makes spall damage nucleation and growth to be dominant at the GBs, indicative of void shapes resembling flat sheets, whereas heat treated samples contained higher concentrations of spherical and oblate ellipsoidal shapes, indicative of transgranular and coalesced spall damage, respectively. Lastly, Escobedo et al. [21] varied the loading history of heat treated copper PCs and discovered a strong relationship between a decrease in tensile stress rate and advanced damage growth and coalescence.

This work aims to provide further insight into how quantitative assessment of spall damage shape using 3D XRT can lead to conclusions on damage mode preference and maturity of spall damage coalescence in two parts: 1) comparing spall damage shapes between shock loaded FCC (Ni) and HCP (Ti) MCs and 2) using spall damage shape fitting to determine the amount of damage growth and coalescence as a function of varying the shock loading kinetics given a constant microstructure.

MATERIALS AND EXPERIMENTAL METHODS

The shock experiments presented in this work are divided into two groups. Group A studies the difference in spall damage shape between pure FCC (Ni) and HCP (Ti) metals. Group B aims to elucidate the effects of loading kinetics on the early stages of damage evolution in shock loaded FCC (Cu) metals. Relevant shock parameters for the plate impact experiments for each group are listed in Tables I and II.

The flyer and target plate materials for Group A were prepared using stock rods of 99.99+% pure Ni and Ti for samples 1A and 2A, respectively. Both materials were heat treated to obtain average grain sizes of approximately 400 μm to ensure the target samples were MCs in order to isolate GB effects on spall damage. Flyer and target plates for experiment 1A were wire cut as circular discs to 8 and 10 mm in diameter and mechanically polished from SiC grit papers through colloidal silica to thicknesses of 500 and 910 μm thick, respectively. Characterization of the heat treated Ti samples revealed an average grain size of 250 μm with a standard deviation of 150 μm, giving a range in grain sizes from 100 to 400 μm. Thus, to ensure the target was a MC, the flyer and target plates for experiment 2A were wire cut as circular discs to 8 and 10 mm in diameter and mechanically polished through a 5:1 ratio of colloidal silica and 30% hydrogen peroxide to thicknesses of 250 and 500 μm, respectively.

Targets in experiment Group A were shock loaded via flyer-plate impact using the TRIDENT laser facility at Los Alamos National Laboratory (LANL). A Nd:glass laser with a fundamental wavelength of 1054 nm illuminated a chemical ablative layer positioned against a plasma shield situated against the flyer plate. A subsequent rapid expansion of plasma and hot gases propelled the flyer into the target plate, resulting in a shock impact akin to gas gun experiments. Additional information on the TRIDENT facility in regards to shock impact studies can be found in [7, 29]. Velocimetry data was recorded throughout the duration of the experiments using VISAR diagnostics. This velocity-time history data was used to calculate the shock pressure and spall strength of the targets shown in Table I based on standard hydrodynamic approximations [3].

The flyer and target plates for Group B were prepared using fully annealed 99.999% pure, oxygen-free high-conductivity (OFHC) copper. Copper targets were prepared as circular discs 15 mm in diameter with varying thicknesses, from 2-6 mm. In order to isolate the effect of loading kinetics controlled by varying the flyer-target thicknesses, the GB

density through the thickness of the targets was kept uniform via heat treatments ranging from 600 °C to 825 °C for 60 to 120 minutes. For additional information regarding the characterization of these heat treatments refer to Escobedo et al. [21].

Table I: Impactor-target shock parameters for Group A.

Sample ID	Target Material	Impactor Velocity (m/s)	σ_{shock} (GPa)	σ_{spall} (GPa)	# of Voids (min. 1,000 Voxels)
1A	Ni	428	9.32	4.64	347
2A	Ti	563	6.93	5.46	886

Table II: Impactor-target geometry and shock parameters for Group B.

Sample ID	Impactor Velocity (m/s) / Thickness (mm)	Target Thickness (mm)	Region under Tension ΔX (mm)	Stress Rate (GPa/μs)	# of Voids (min. 1,000 Voxels)
1B	91 / 1.0	2.0	1.01	35	22
2B	90 / 1.0	4.0	1.68	25	269
3B	91 / 1.5	3.0	1.25	24	409
4B	92 / 1.5	5.0	1.48	20	450
5B	92 / 2.5	4.0	1.59	19	363
6B	92 / 2.5	6.0	1.73	17	185

Plate impact experiments were conducted on Group B using a 40 mm bore light gas gun. The copper samples were press-fit into target assemblies consisting of three concentric momentum trapping rings to prevent lateral release waves from interfering with the spall plane. Similar to Group A, free surface velocity profiles were obtained for all samples in Group B using VISAR probes. Further experimental details for similar experimental conditions can be found in [20]. All experiments were conducted two to three times to ensure repeatability and to generate additional statistics of damage distributions. The peak compressive shock stress was held consistent at ~1.5 GPa to ensure that the spall damage was confined to incipient stage of damage development to study directly how the tensile stress rate affects spall growth and coalescence. Samples 1B-6B were chosen as representatives for their respective shock loading conditions in this work. The last two columns in Table II, the through-thickness area subjected to the tensile release pulse and the tensile stress rate, were calculated using a hydrodynamic code for each experiment [21].

X-ray tomography was performed on the central regions of the spall planes for all samples in experimental Groups A and B. Rectangular sections with a 1 mm x 1 mm cross-section were exhumed from the samples in Group A, whereas ~2 mm diameter cylindrical

cross-sections were exhumed from the samples in Group B. X-ray tomography was performed on the exhumed sections from Group A at the Advanced Photon Source (APS) at Argonne National Laboratory on beamline 2-BM with a resolution of ~ 0.65 μm per pixel, whereas samples from Group B were scanned at Los Alamos National Laboratory (LANL) with a resolution of ~ 2.24 μm per pixel. Beam conditions for The APS and LANL may be found in [10] and [30], respectively. It was determined by Patterson et al. [30] that a minimum 1,000 voxels (cubic pixels) are required for maintaining less than 10% absolute error for accurately rendering the shape of an object, thus all XRT datasets were sieved to a minimum of 1,000 voxels for the shape fitting analysis used in this work. For volumetric analysis a sieve of 120 voxels was also performed [30]. All XRT datasets underwent careful smoothing and thresholding processes before applying volumetric sieve or labelling modules. Voids appearing at the edges of the dataset were removed in the software using a "border kill" function, as these features may not be properly characterized by total volume or shape.

The moments of inertia are mathematical properties that are determined by the shape and volume distribution in 2D or 3D space with respect to a reference axis [31]. The Avizo® software package was used to obtain the full inertia tensor of each spall damage site of at least 1,000 voxels in volume for each dataset. Each inertia tensor may be used to fit individual voids to a best fit ellipsoid for spall damage analysis. Solving for the semi-axes governing these ellipsoidal shapes requires taking the full inertia tensor for each individual void, finding the principal moments of inertia, and applying the following appropriate relationship to solve for the ellipsoid's semi-axis based on how Avizo® defines the inertia tensor [32]:

$$M_{2z} = \frac{1}{5} M c^2 \quad (1)$$

Where M_{2z} is the principal moment of inertia about the z-axis, M is the volume of the object, and c is the ellipsoid semi-axes corresponding to the z-axis. Cyclical substitution of x and y into Eq. 1 is required to relate the principal moments M_{2x} to semi-axis a and M_{2y} to semi-axis b. For emphasis, the typical relationships between the principal moments and ellipsoid semi-axes are proportional to the sum of the squares of the other two semi-axes terms as explained in Wang et al. [31], however, Eq. 1 is obtained by correctly solving the moments as defined by the software [32] and whose derivation is further detailed in [18, 19]. The convention used in this work for relating the principal moments of inertia to the semi-axes of best fit ellipsoids will always be defined as $c \geq b \geq a$.

The volume term, M, was considered irrelevant to the analysis process because the ratios of the semi-axes a/c and b/c were used to quantify void shapes. However, the volume weighted average on the global average semi-axes aspect ratio pairs a/c and b/c has been considered in this work:

$$\overline{AR} = \frac{\sum V_i AR_i}{\sum V_i} \quad (2)$$

where AR_i and V_i are the semi-axis ratios a/c or b/c and the volume of each void in the dataset, respectively. The volume weighted average aspect ratio gives insight into the effects of shock loading kinetics on the extent of spall damage growth and coalescence.

RESULTS AND DISCUSSION

Spall Damage Shape Analysis for FCC vs. HCP Multicrystals

Experimental Group A compares the shape of spall damage between a shock loaded FCC (Ni) and HCP (Ti) MCs. Although it is well documented that transgranular spall damage nucleates as octahedral voids in FCC metals [33], there are relatively few fundamental spall damage studies on HCP materials [27], particularly high-purity Ti. Inspection of the thresholded and sieved 3D XRT renderings provide for a quick qualitative analysis of the central spall regions for samples 1A and 2A, shown in Fig. 1. It can be seen that in the Ni sample, 1A, incipient spherical voids are scattered throughout the entire dataset with the largest voids appearing to be flat, sheet like voids. This has previously been shown to be indicative of trans- and intergranular voids present in shock loaded Cu PCs [9, 10, 18, 19] with large volume sheet-like intergranular voids appearing at intrinsic weak GBs in Cu MCs [14]. The intermediate volume voids appear to exist as "string of pearls," indicative of coalesced damage sites in classic FCC ductile spall failure.

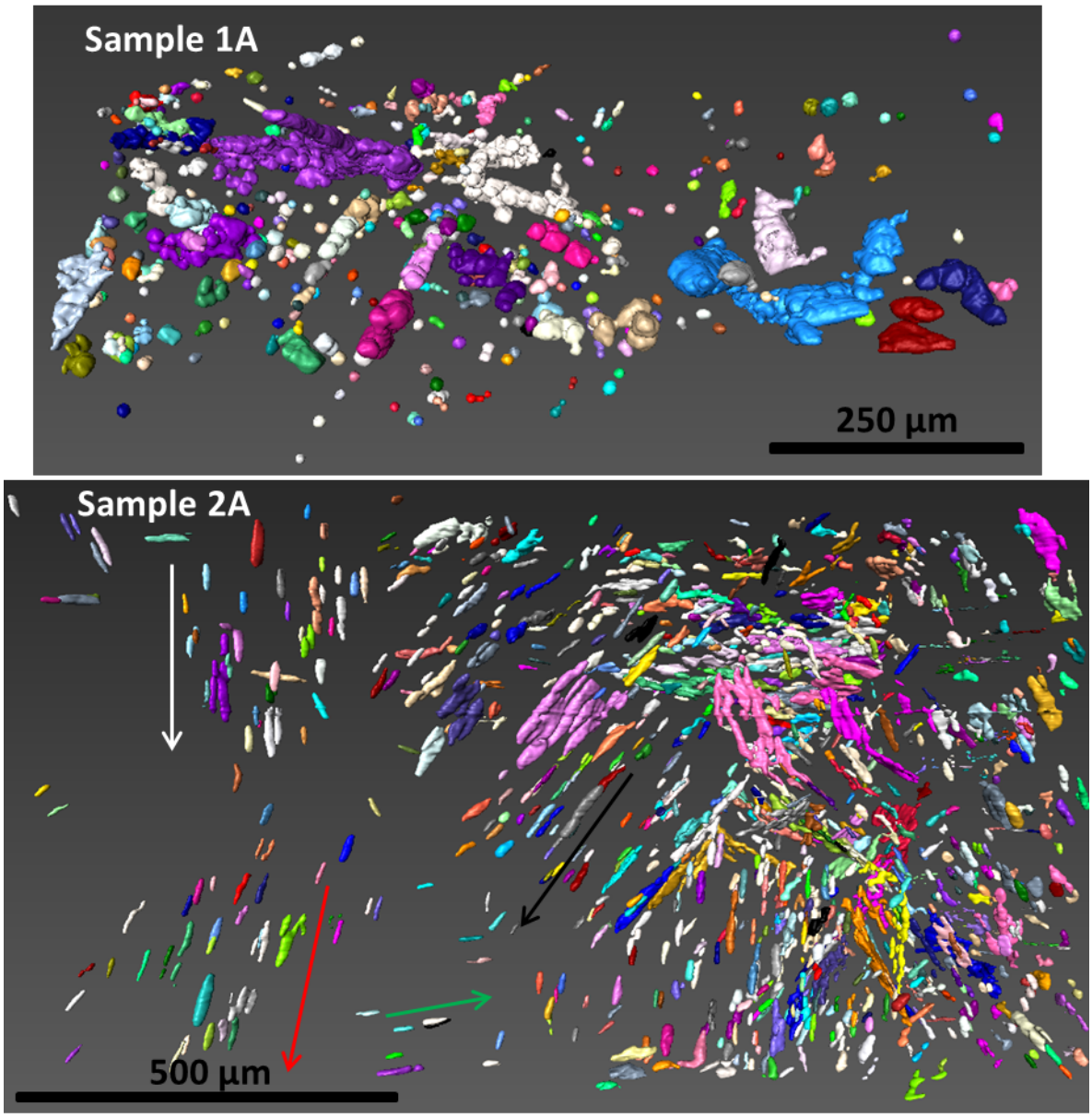

Fig. 1: Spall damage renderings from 3D XRT data for samples 1A (Ni) and 2A (Ti). Arrows shown in the rendering for sample 2A indicate preferred transgranular damage orientations. The shock direction is vertical for 1A and out of the page for 2A. All colors are for visual aide only.

Visual inspection of sample 2A provides a stark contrast in the nucleation, growth, and coalescence processes between FCC and HCP materials. Most all of the voids in sample 2A appear to be lenticular in shape. Unlike shocked FCC materials, this is not necessarily an indication of void coalescence, but rather a result of the preferred nucleation and growth process, the latter of which is fundamentally driven by crystal plasticity. In HCP materials deformation is restricted by their low structural symmetry, thus providing fewer slip systems available to nucleate damage when compared to their FCC counterparts [24]. This is the likely explanation for the shape and orientation of the lenticular spall damage seen in sample 2A. Note that there are volumetric regions on the same order of magnitude as the material's average grain size within the global dataset where the spall damage has clear orientation dependence, as indicated by the arrows in Fig. 1. Further characterization must be performed using electron backscattering diffraction of serial sections through the thickness of this sample to elucidate if these directions correspond to preference to basal, prismatic and/or pyramidal plane-Burgers vector slip systems within each grain. Such analysis is beyond the scope of the work presented here, but would prove invaluable for further understanding spall damage kinetics in pure HCP metals. Furthermore, it is also clear in Fig. 1 that large volume coalesced damage sites simply appear as conjoined adjacent lenticular damage sites.

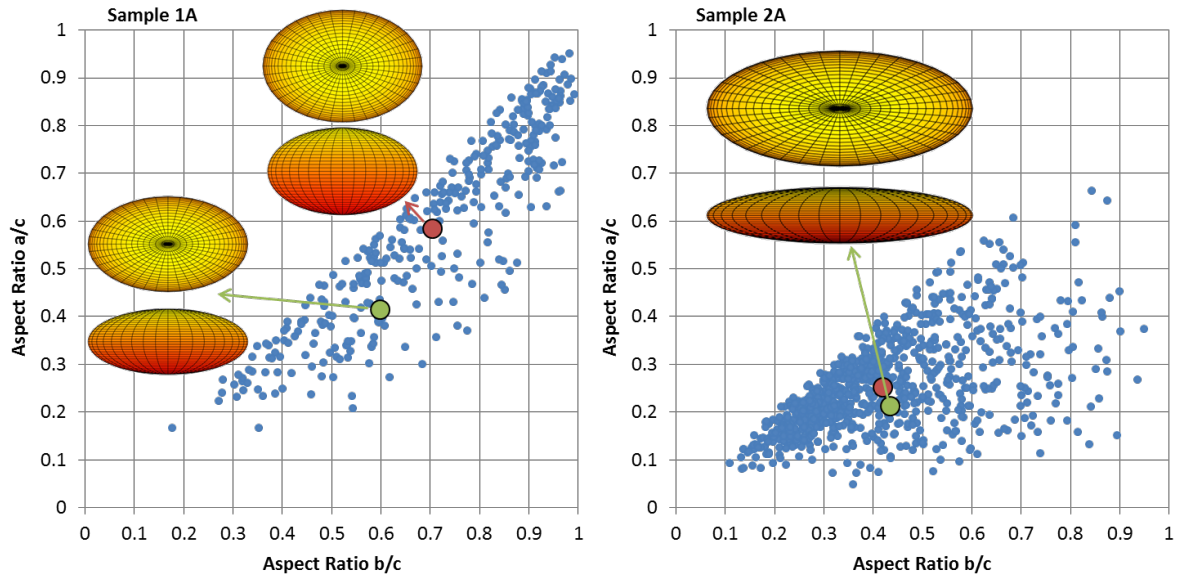

Fig. 2: Best fit ellipsoid semi-axes ratio plots for samples 1A and 2A. The average and volume weighted average semi-axes ratio pairs are represented by the red and green circles, respectively. Aspect ratio *b*-*c* and *a*-*c* planar views are shown for visual aide.

Each void underwent the process outlined in the previous section for fitting its full moment of inertia tensor to a representative ellipsoid with aspect ratios *a*/*c* and *b*/*c*. As both *a*/*c* and *b*/*c* approach unity the resulting shape is a sphere, as *a*/*c* approaches 0 and *b*/*c* approaches unity the resulting shape is a flattened disk, and as both *a*/*c* and *b*/*c* approach 0 the resulting shape is an elongated needle. Fig. 2 contains scatter plots of aspect ratios *a*/*c* vs. *b*/*c* for all voids above the 1,000 voxel sieve for samples 1A and 2A. An important feature of

Fig. 2 is the incorporation of a volume weighted average aspect ratio pair found by utilizing Eq. 2 for each dataset.

Since spall damage growth is controlled by crystal plasticity, incipient transgranular damage sites may not grow isotropically, rather they are likely grow within grains that contain a high number of slips systems with respect to the loading direction. For FCC metals these plastically-driven growth mechanisms lead to a transition from spall damage nucleation, where both aspect ratio pairs are approximately unity, to a regime dominated by void growth, where both aspect ratio pairs may decrease to around 0.5-0.6 due to anisotropic effects. The regime dominated by void coalescence exists where the aspect ratio pairs further decrease for one or both aspect ratios. Quantitatively assigning a void as either newly coalesced or heavily grown along a preferred crystallographic direction is impossible to discern with absolute certainty without additional microscopy analysis and/or individual void inspection of the tomography renderings.

There is a noticeable difference in the locations of the unweighted average (red circle) and volume weighted average (green circle) aspect ratio pairs in the Ni sample 1A, as shown in Fig. 2. The unweighted average lies in the regime where the aspect ratio pairs would indicate transgranular damage that has exhibited some amount of growth in FCC metals. The volume weighted average shifts a significant amount to within the region indicative of intergranular damage and coalesced damage dominance. Although there are fewer voids within this coalescence dominated region, the drastic shift in the unweighted vs. weighted aspect ratio pairs indicates that the voids that have coalesced are much larger than the incipiently nucleated voids and voids exhibiting varying degrees of growth. It is highly likely that these large volume damage sites are present along the GBs, which act as the intrinsic weak links within the MC structure and matches well with other studies of spall damage in Cu MCs [14].

Consistent with visual inspection, Fig. 2 shows that indeed most voids present in the Ti sample 2A are lenticular, or, needle-like in shape. The difference in the unweighted and weighted average aspect ratio pair is negligible when compared to the Ni sample 1A. This indicates that the larger volume voids are roughly the same shape as most of the voids within the dataset. The slight shift is to the right and downwards on the a/c vs. b/c aspect ratio plot, which is indicative of intergranular damage regardless of the crystal structure, as damage sites will follow a GB through the thickness of the material. The small magnitude of the shift also indicates that the coalesced voids or damage present at the GBs have not grown many times larger than the average void volume, thus the spall damage is heavily incipient. The dominant lenticular void shape has been seen in shock studies on Ti alloys [24-28], matching the results presented here.

Lastly, the extent of growth of the large volume damage sites is affected by the magnitude of the compressive shock stress. From Table I it is clear that the Ni sample 1A underwent a higher peak compressive shock stress in relation to its spall strength in comparison to the Ti sample 2A. Further XRT and microstructural analysis are required for a suite of shock loading conditions to fully understand the spall damage nucleation and growth kinetics as a function of spall damage shape in FCC vs. HCP materials.

Spall Damage Shape as a Function of Shock Loading Kinetics in Copper

The premise of experimental Group B is to further elucidate the relationship between shock loading kinetics by changing the tensile stress loading rate and maintaining consistent peak compressive shock stresses and volume of microstructural defects in the Cu PCs. Fig. 3 shows the XRT renderings of the 1,000 voxel sieved datasets for all six shock experiments in Group B. From visual inspection there appears to be an increase in void growth and

coalescence from sample 1B through sample 6B. As the sample number increases the tensile stress rate decreases. In other words, the duration of the tensile release pulse is increased, which may allow for a longer period of time for incipient spall damage to grow and coalesce. Immediately, there appears to be an inverse relationship between void growth maturity and tensile stress rate, which is consistent with preliminary findings in Escobedo et al. [21].

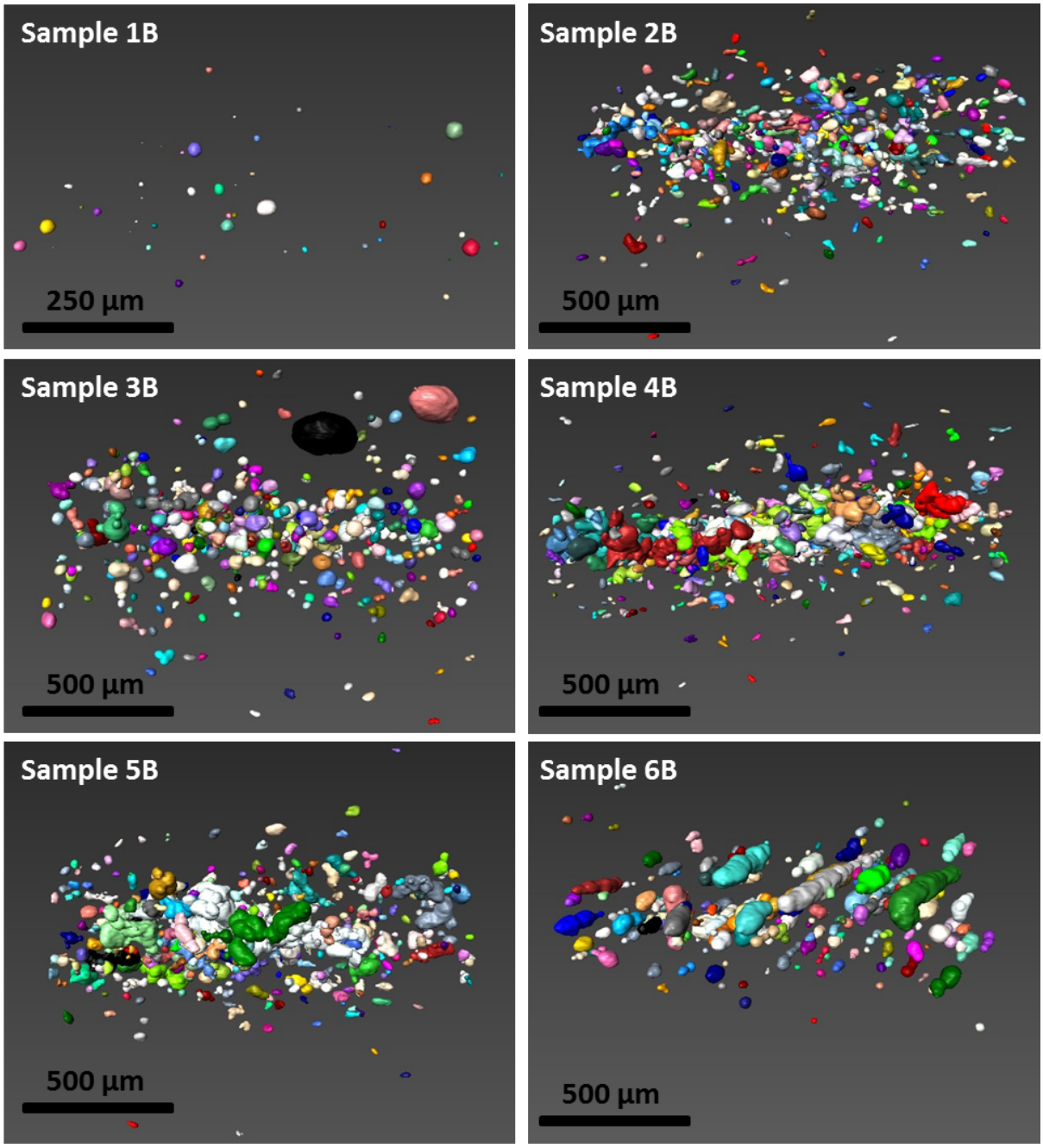

Fig. 3: Spall damage renderings from 3D XRT data for samples in Group B. The shock direction is vertical for all samples and the colors are for visual aide only.

Fig. 4 plots the volume weighted average aspect ratio pair for each experiment. It appears that as the stress rate decreases the volume weighted average aspect ratio pair decreases from regions of void nucleation, to nucleation and growth, to growth and dominate coalescence. Samples 2B and 3B appear to be "swapped" with one another based on this

trend. Upon further visual inspection of the XRT renderings it is clear that there are a few very large voids that have exhibited significant growth while maintaining a high aspect ratio pair in sample 3B, however; from Fig. 5d it is clear that the difference in the unweighted vs. volume weighted aspect ratio pairs is low for samples 2B and above the predicted trendline for 3B. This indicates little difference in the most common void shapes and the larger volume void shapes for 2B, but not 3B. It appears as though sample 3B has experienced a higher degree of individual void growth rather than transitioning to coalescence. Furthermore, it can be seen from Fig. 5b that the equivalent average void diameter increases with decreasing tensile stress rate, meaning that the incipient damage in sample 2B are not as spherical as one would expect given previous studies on transgranular void nucleation experiencing little growth in FCC metals [10, 18, 33].

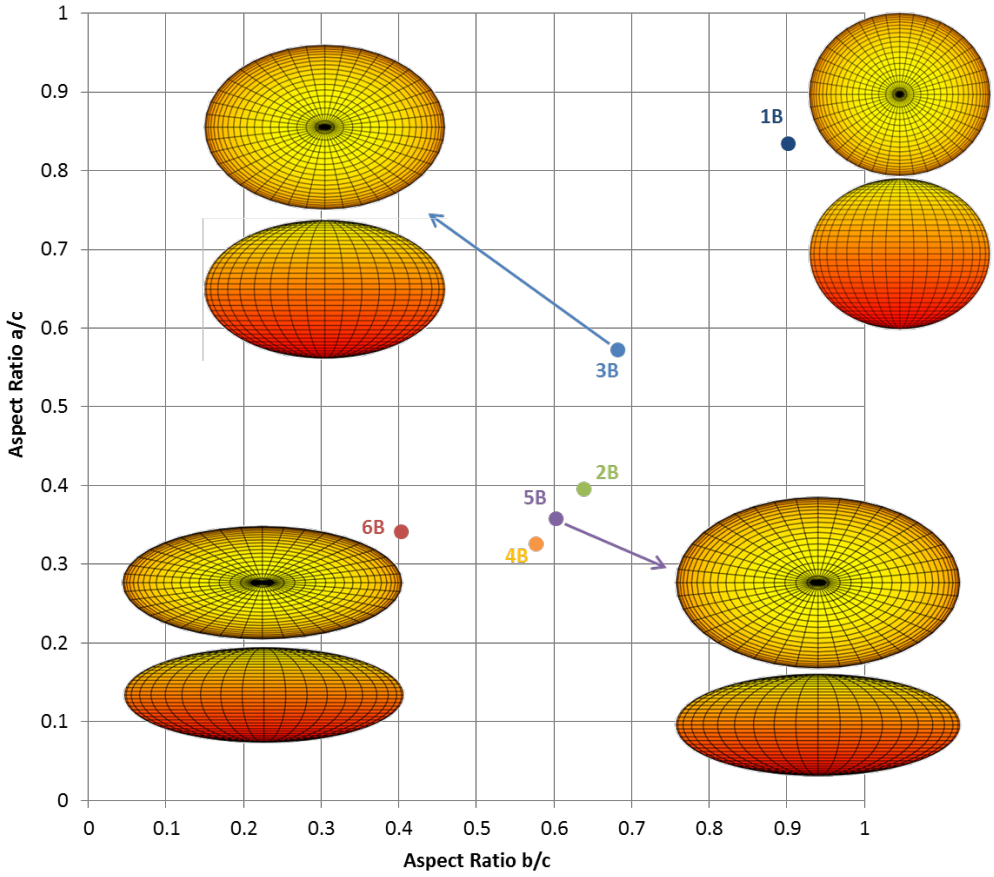

Fig. 4: Best fit volume weighted average semi-axes ratio pairs *a*/*c* vs. *b*/*c* for all samples in Group B. Clockwise from the top-left: aspect ratio *b*-*c* and *a*-*c* planar views are shown for samples 3B, 1B, 5B, and 6B.

Several overall trends, that are inter-related, are observed from the plots in Fig. 5. From Fig. 5a it is clear that as the volume weighted ellipsoid aspect ratio pairs *a*/*c* and *b*/*c* decrease the equivalent void diameter increases, confirming that void volumes increase as such change in shape indicates a transition from spall damage nucleation, to nucleation and growth, to coalescence. Fig. 5b illustrates a well-defined relationship between a decrease in stress rate leading to an increase in equivalent void diameter, which is in good agreement with spall damage area fractions increasing with decreasing stress rate reported by Escobedo et al. [21]. Another trend as shown in Fig. 5c is a decrease in tensile stress rate leads to a decrease in the volume weighted average aspect ratio pairs. This supports the observations that low tensile stress rates lead to larger volume voids via growth and, in turn, dominated by coalescence. Lastly, Fig. 5d shows that as the tensile stress rate decreases there is an

increasing difference in weighted vs. unweighted aspect ratio pairs. This indicates that spall damage sites that are heavily coalesced make up a larger volume fraction of the overall dataset. Furthermore, the difference in unweighted vs. weighted aspect ratio pairs *a*/*c* and *b*/*c* begin to diverge for the lower tensile stress rates of 19 and 20 GPa/μs. These lower stress rate samples, 4B and 5B, each exhibit a low *b*/*c* aspect ratio difference as compared to the a/*c* aspect ratio, indicating that the larger volume voids are indeed biased towards flattened and lenticular ellipsoids.

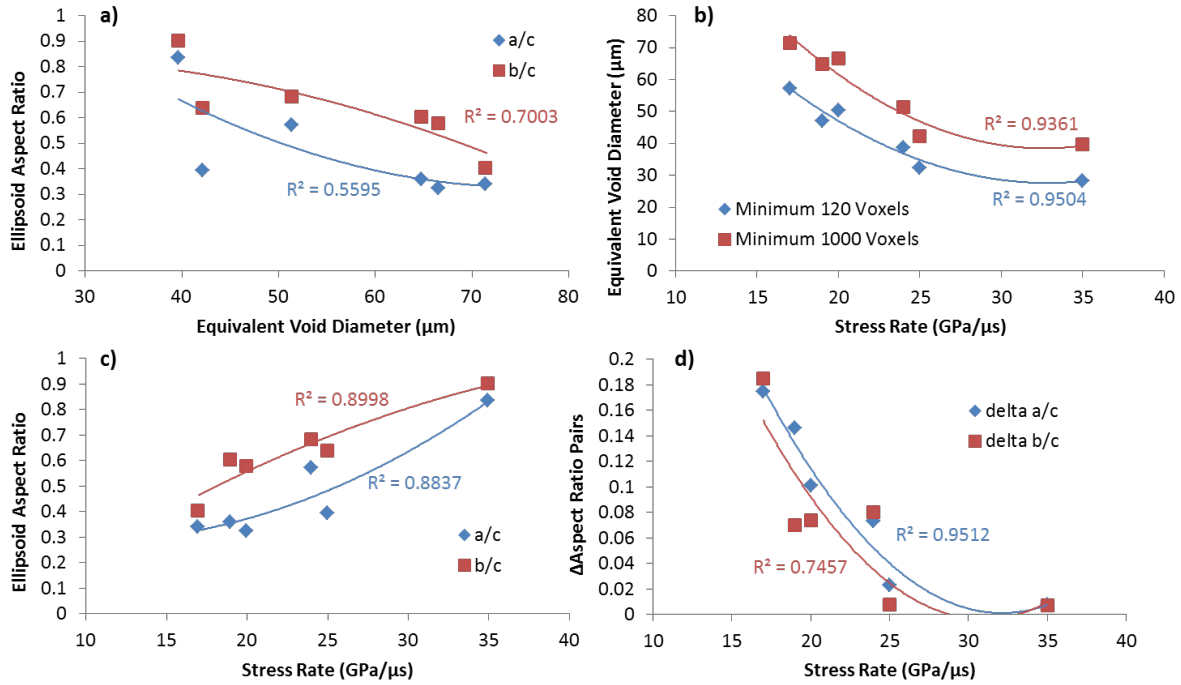

Fig. 5: XRT void statistics from samples 1B-6B comparing best fit ellipsoid aspect ratios, tensile stress rate, equivalent void diameter, and differences in weighted and unweighted aspect ratio pairs. All trendline fits are 2nd order polynomials.

However, for sample 6B, which has the lowest stress rate of 17 GPa/μs, again has convergence in the difference between unweighted vs. weighted aspect ratio pairs *a*/*c* and *b*/*c*. This could indicate that at a threshold tensile stress rate less voids initially nucleate due to elastic-plastic inhibition zones surrounding nucleated voids [34]. Referring back to Table II this also follows the trend that there exists a peak in the number of damage sites near the middle of the tensile loading rates and decreases towards the minimum stress rate of 17 GPa/μs, which also infers coalescence as the dominant damage mode at lower stress rates. The voids that did nucleate would then be allowed longer time duration to grow and fully coalesce. This could potentially explain the very unique large volume "string of pearls" damage sites present in sample 6B, but experiments at even lower stress rates coupled with appropriate finite element and molecular dynamics would be necessary to explore the kinetics of such phenomenon.

CONCLUSIONS

A methodology has been laid out for utilizing 3D XRT data to aide in quantifying relationships between spall damage nucleation, growth, and coalescence processes across a range of shock loaded materials and experimental conditions based on ellipsoidal shape fitting of individual damage sites. Since this process is nondestructive for user-defined

regions of interest it lends itself to finding regions of particular interest within the sample prior any sort of additional sectioning and also may provide information for computational models. Preliminary conclusions drawn from this work in addition to providing an outline for a successful characterization method include:

- It was clearly demonstrated that the shape fitting process was able to quantitatively provide information regarding the preferred shapes of incipiently nucleated spall damage in shock loaded pure FCC (Ni) and HCP (Ti) multicrystals; spherical for FCC and lenticular for HCP.
- Applying a volumetric weighted average for the best fit ellipsoid semi-axes ratio pairs *a*/*c* and *b*/*c* was able to determine that the Ni sample's coalesced voids are much larger in volume than voids with shapes indicating nucleation and moderate growth. These sites likely occurred at GBs, similar to findings previously reported [14].
- There was little shift in the weighted averaging of the semi-axes ratio pairs in the shock loaded Ti sample, indicating that the dominant lenticular void shape is within the nucleation to nucleation and growth regimes of damage kinetics. Additionally, the damage was oriented along specific directions at intervals on the same order as the average grain size, requiring additional investigation into what potentially slip plane traces these follow.
- From a suite of shock experiments on pure Cu polycrystals it has been confirmed that as the applied tensile stress rate decreases, the degree of spall damage growth and coalescence increases.
- The void shapes seem to indicate that there may be statistically reliable thresholds for transitions between spall damage nucleation, nucleation and dominate growth, and growth and dominate coalescence as the stress rate decreases for identical material conditions. Additional datasets would be required to deduce these thresholds.

ACKNOWLEDGEMENTS

This research work was funded by LANL under LDRD #20060021DR, LDRD-DR #20100026 and by the Department of Energy, NNSA, under SSAA Grants #DE-FG52-06NA26169, DE-FG52-10NA29653, DE-NA0002005 and DE-NA0002917 and APS General User Proposal 35561. Los Alamos National Laboratory is operated by LANS, LLC, for the NNSA of the US Department of Energy under contract DE-AC52-06NA25396. Eric Loomis, Pat Dickerson (LANL), Damian Swift (LLNL), David Wright, and Dallas Kingsbury (ASU) are thanked for their help during the various phases of the research work. Access to the TRIDENT Facility & Electron Microscopy Laboratory at LANL, Pavel Shevchenko at APS 2-BM, as well as the Center for High Resolution Electron Microscopy and the Mechanical Testing Laboratory at ASU is gratefully acknowledged.

REFERENCES

[1] D.R. Curran, L. Seaman, D.A. Shockey, "Dynamic Failure of Solids," *Physics* Reports, 147 (5 & 6) (1987), 253-388.
[2] D.E. Grady, "The Spall Strength of Condensed Matter," *Journal of the Mechanics and Physics of Solids*, 36 (3) (1988), 353-384.
[3] M.A. Meyers, *Dynamic Behavior of Materials* (John Wiley & Sons, New York, 1994).
[4] R.W. Minich et al., "Effect of Microstructural Length Scales on Spall Behavior of Copper," *Metallurgical and Materials Transactions A*, 35 (A) (2004), 2263-2673.
[5] B.L. Henrie et al., "Investigating Inciepiently Spalled Tantalum through Multiple Planes and Serial Sectioning," *AIP Conference Proceedings*, 845 (2005), 627.

[6] Czarnota et al., “Modelling of Dynamic Ductile Fracture and Application to the Simulation of Plate Impact Tests on Tantalum,” *Journal of the Mechanics and Physics of Solids*, 56 (2008), 1624-1650.
[7] P. Peralta et al., “Characterization of Incipient Spall Damage in Shocked Copper Multicrystals,” *International Journal of Damage* Mechanics, 18 (2009), 393-413.
[8] L. Wayne et al., “Statistics of Weak Grain Boundaries for Spall Damage in Polycrystalline Copper,” *Scripta Materialia*, 63 (2010), 1065-1068.
[9] A.D. Brown et al., “3-D Characterization of Global and Local Microstructural Effects on Spall Damage in Shock Loaded FCC Metals: Experimental and Modeling,” *ASME Int., Mechanics of Solids, Structures and Fluids*, IMECE2013-65642 (2013), V009T10A033.
[10] A.D. Brown et al., “Microstructural Effects on Damage Nucleation in Shock-Loaded Polycrystalline Copper,” *Metallurgical and Materials Transactions A*, 46 (10) (2015), 4539-4547.
[11] J.P. Escobedo-Diaz, “Effects of Grain Size and Boundary Structure on the Dynamic Tensile Response of Copper,” *Journal of Applied Physics*, 110 (2011), 033513.
[12] E.K. Cerreta et al., “Early Stage Dynamic Damage and the Role of Grain Boundary Type,” *Scripta Materialia*, 66 (2012), 638-641.
[13] J.P. Escobedo, E.K. Cerreta, D. Dennis-Koller, “Effect of Crystalline Structure on Intergranular Failure during Shock Loading,” *JOM*, 66 (1) (2014), 156-164.
[14] K. Krishnan et al., “Three-Dimensional Characterization and Modeling of Microstructural Weak Links for Spall Damage in FCC Metals,” *Metallurgical and Materials Transactions A*, 46 (10), 4527-4538.
[15] S.J. Fensin et al., “Effect of Loading Direction on Grain Boundary Failure Under Shock Loading,” *Acta Materialia*, 64 (2014), 113-122.
[16] Escobedo, J. P., E. K. Cerreta, and D. Dennis-Koller. "Effect of crystalline structure on intergranular failure during shock loading." *JOM* 66.1 (2014): 156-164.
[17] Lieberman, Evan J., et al. "Microstructural effects on damage evolution in shocked copper polycrystals." *Acta Materialia* 116 (2016): 270-280.
[18] Brown, A. D., et al. "Correlations Between Spall Damage Mode Preference and Microstructure in Shocked Polycrystalline Copper: A 3-D X-Ray Tomography Study." *Journal of Dynamic Behavior of Materials* 1.4 (2015): 388-396.
[19] Brown, A. D., et al. "Methodology for Determining Spall Damage Mode Preference in Shocked FCC Polycrystalline Metals from 3D X-Ray Tomography Data." *Characterization of Minerals, Metals, and Materials 2016*: 57-64.
[20] Dennis-Koller, D., et al. "Isolation of kinetic and spatial properties of uni-axial dynamic tensile loading of OFHC copper." *EPJ Web of Conferences*. Vol. 26. EDP Sciences, 2012.
[21] J.P. Escobedo et al., “Influence of Shock Loading Kinetics on the Spall Response of Copper,” *Journal of Physics: Conference* Series, 500 (11) (2014).
[22] Yang, Yang, et al. "Multidimensional Study on Spall Behavior of High-Purity Copper Under Sliding Detonation." *Metallurgical and Materials Transactions A* 46.9 (2015): 4070-4077.
[23] Yang, Yang, et al. "Spall behaviors of high purity copper under sweeping detonation." *Materials Science and Engineering: A* 651 (2016): 636-645.
[24] Hazell, P. J., et al. "The shock and spall response of three industrially important hexagonal close-packed metals: magnesium, titanium and zirconium." *Phil. Trans. R. Soc. A* 372.2023 (2014): 20130204.
[25] Boidin, X., et al. "Identification of damage mechanism and validation of a fracture model based on mesoscale approach in spalling of titanium alloy."*International journal of solids and structures* 43.14 (2006): 4595-4615.

[26] Tyler, C., J. C. F. Millett, and N. K. Bourne. "Spallation in Ti-6Al-4V: Stress Measurements and Recovery." *SHOCK COMPRESSION OF CONDENSED MATTER-2005: Proceedings of the Conference of the American Physical Society Topical Group on Shock Compression of Condensed Matter*. Vol. 845. No. 1. AIP Publishing, 2006.
[27] McDonald, Samuel A., et al. "Spallation response of Ti-6Al-4V: Rear surface velocimetry and X-ray tomography." *SHOCK COMPRESSION OF CONDENSED MATTER-2011: Proceedings of the Conference of the American Physical Society Topical Group on Shock Compression of Condensed Matter*. Vol. 1426. No. 1. AIP Publishing, 2012.
[28] Ren, Yu, et al. "Shock-induced mechanical response and spall fracture behavior of an extra-low interstitial grade Ti–6Al–4V alloy." *Materials Science and Engineering: A* 578 (2013): 247-255.
[29] Paisley, D. L., et al. "EXPERIMENTAL METHOD FOR LASER-DRIVEN FLYER PLATES FOR 1-D SHOCKS." *SHOCK COMPRESSION OF CONDENSED MATTER-2007: Proceedings of the Conference of the American Physical Society Topical Group on Shock Compression of Condensed Matter*. Vol. 955. No. 1. AIP Publishing, 2007.
[30] B.M. Patterson et al., "Dimensional Quantification of Embedded Voids or Objects in Three Dimensions using X-ray Tomography," *Microscopy and Microanalysis*, 18 (2012), 390-398.
[31] L. Wang, Y.J. Park, Y. Fu, "Representation of Real Particles for DEM Simulation using X-ray Tomography," *Construction and Building Materials*, 21 (2007), 338-346.
[32] Avizo® 8 Reference Guide (2013).
[33] A.L. Stevens, L. Davison, W.E. Warren, "Spall Fracture in Aluminum Monocrystals: A Dislocation Dynamics Approach," *Journal of Applied Physics*, 43 (1972), 4922-4927.
[34] Trumel, Hervé, et al. "On probabilistic aspects in the dynamic degradation of ductile materials." *Journal of the Mechanics and Physics of Solids* 57.12 (2009): 1980-1998.